NGU Report 2009.037
Electrical resistivity and refraction seismic data acquisition over a segment of the Møre-Trøndelag Fault Complex

Geological Survey of Norway
NO-7491 Trondheim, Norway
Tel.: 47 73 90 40 00
Telefax 47 73 92 16 20

REPORT

Report no.: 2009.037 | ISSN 0800-3416 | Grading: Open

Title:
Electrical resistivity and refraction seismic data acquisition over a segment of the Møre-Trøndelag Fault Complex

Authors:
Aziz Nasuti, Kurdistan Chawshin, Einar Dalsegg, Jan Fredrik Tønnesen, Jörg Ebbing and Jomar Gellein

Client:

County:
Sunndalsøra

Commune:
Møre-Romsdal

Map-sheet name (M=1:250.000)

Map-sheet no. and -name (M=1:50.000)
1320 and 1420

Deposit name and grid-reference:

Number of pages: 36 Price (NOK): 135,-
Map enclosures:

Fieldwork carried out:	Date of report:	Project no.:	Person responsible:
10/2007, 06/2008	10/09/2010	3184.00	

Summary:

The Møre-Trøndelag Fault Complex (MTFC) is a key structural element in mid-Norway. 2D resistivity profiling and shallow refraction seismics have been carried out to resolve the near surface structures of the fault in the area of Tingvollfjorden. Here two of the main segments of the MTFC are evidenced by the topography (Tjellefjorden Fault and Fannefjorden Fault). In total a series of seven resistivity profiles and one refraction profile will be presented in this report. The resistivity profiles reveal very low resistive zones in the bedrock. The geometries of the low resistivity zones strongly suggest a highly fractured bedrock. Along one of the resistivity profiles, additionally a shallow refraction seismic profile was conducted. In addition, the refraction profile shows three distinct low velocity anomalies in the bedrock, which might relate to damage zones of the MTFC. Comparison between the 2D resistivity and refraction seismic shows that two weak zones correlate, while the third velocity zone is probably artifact.

Keywords:	2D Resistivity	Refraction seismic
Møre-Trondelag Fault Complex	Tingvollfjorden	Tjellefjorden Fault
Fannefjorden Fault		

CONTENTS

FIGURES

TABLES

1 INTRODUCTION

We present a series of 2D resistivity and shallow refraction seismic surveys in the area around Tingvoll, where two segments of the Møre–Trøndelag Fault Complex (MTFC) are supposed to exist. The aim is to detect the faults at the near subsurface by using these methods and get detailed information about the dip and exact location of the Tjellefjorden and Fannefjorden faults (Fig. 1.1). The MTFC is of interest, as normal-sense reactivation of inherited structures along much of coastal Norway suggests a structural link between the processes that destroy today's mountains and those that created them (Redfield & Osmundsen, 2009). The Paleozoic Møre–Trøndelag Fault Complex (MTFC) was reactivated as a normal fault during the Mesozoic and, probably, throughout the Cenozoic until the present day. It strikes ENE-WSW, paralleling the coastline of south central Norway, and separates the northern North Sea basin system from the deep Mesozoic Møre and Vøring Basins (Redfield et al., 2005) (Fig. 1). Well-preserved kinematic indicators and multiple generations of fault products are exposed along the Tjellefonna fault, a well-defined structural and topographic lineament parallel to both the Langfjorden and the ``Great Escarpment``. The slope instability that was formerly present at Tjelle, and additional instabilities currently present throughout the region, may be viewed as the direct product of past and ongoing development of tectonic topography in mid-Norway (Redfield & Osmundsen, 2009).

Geophysical methods such as 2D resistivity and shallow refraction seismics can be used to map fracturing and faulting. Shallow refraction seismics is the common method to detect fractures in the bedrock and active faults. Also, resistivity studies can image structures with high resolution at shallow depths.

Refraction seismics is generally very effective at determining bedrock depths since bedrock usually has a higher velocity than the overburden. Furthermore, with refraction seismics we are able to provide fairly detailed lateral velocity variations since depth estimates can be made below each geophone. Refraction seismics have limited possibilities provides energy to large depth in the bedrock. For the resistivity, new techniques make it possible to delineate the 2D resistivity distribution down to approximately 130 meters, and to characterize the fault/fracture zones with respect to hydrogeology and mineral content (Rønning et al. 2003). Fractures

increase the secondary porosity of bedrock, and since the bedrock is normally water-saturated, the result is usually a reduced resistivity.

Joint together, these two methods are of prime importance when welding surface mapping with deep geophysics. In the reminder of this report, we will present the data acquisition and some first-order interpretations.

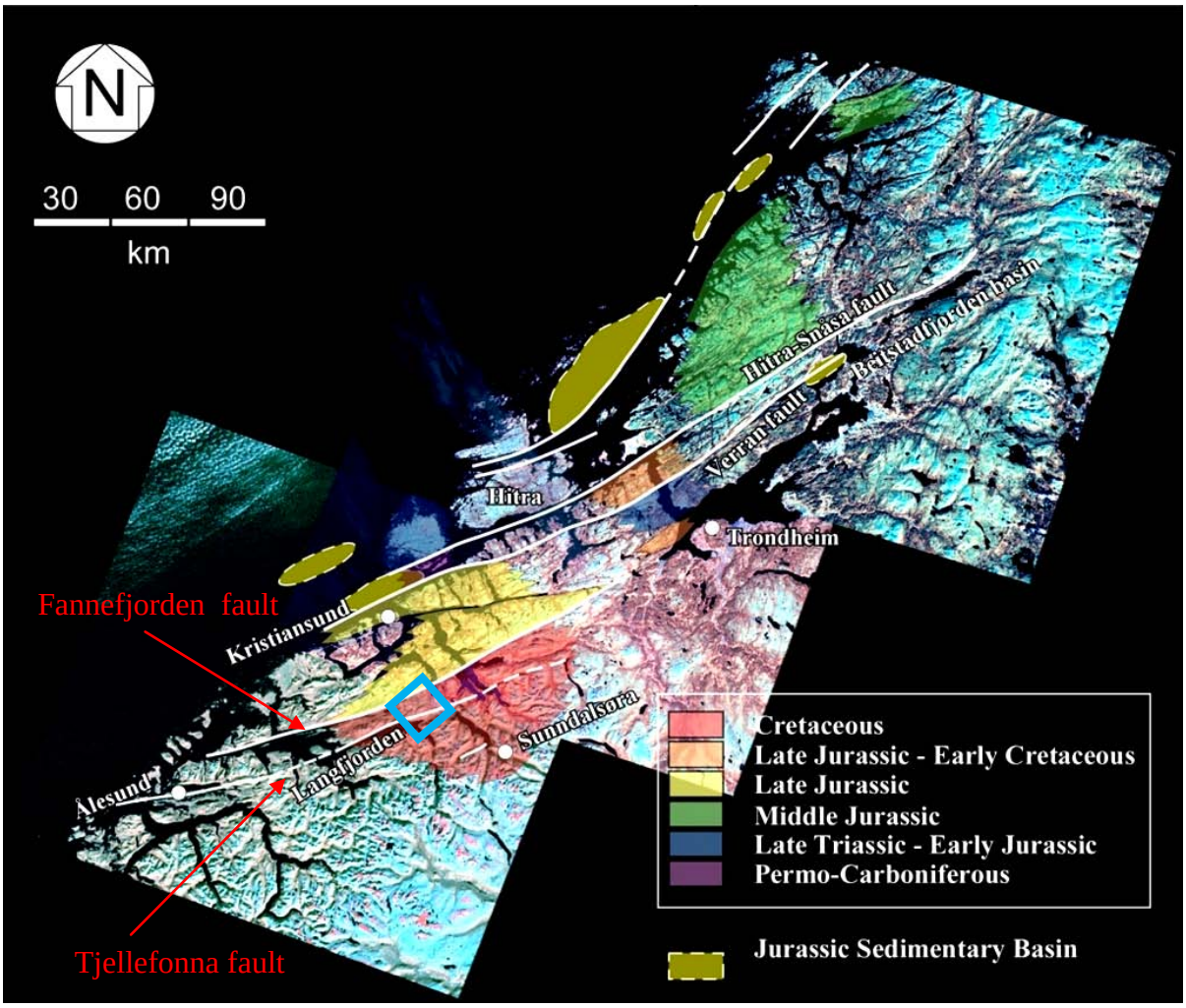

Figure 1.1 *Principal structural features of the Møre-Trøndelag Fault Complex (MTFC) and surrounding regions (modified from Redfield et al, 2005).The study area is framed in blue.*

2 2D RESISTIVITY IMAGING

2D resistivity imaging, as one geoelectrical imaging technique, is one of the geophysical methods often applied in an early stage of ground investigations to get a first-order idea of the shallow subsurface (Dahlin et al., 1999; Rønning, 2003; Ganerød et al., 2006). The advantage of the method is, that measurements are relatively fast and cost efficiently compared to other profiling methods (e.g. refraction seismics). In order to interpret the data, certain knowledge of the geological setting of the area is important. Geoelectrical imaging is used for measuring the spatial variation in subsurface resistivity. Resistivity of the different geological materials differs greatly from about 10^{-6} Ωm in minerals such as graphite to more than 10^{12} Ωm for dry quartzitic rocks (Reynolds 1997). Most rock-forming minerals are insulators. So the resistivity of crystalline rocks depends largely on the amount and quality of water present and the degree of weathering of the rock. Therefore, a rock without water-bearing fractures or weathering has a high resistivity whereas clay-weathered rock or rock with water-bearing fractures has a considerably lower resistivity (Parasnis 1997, Binley & Kemna 2005).

When electrical resistivity measurements are made, a direct current is transmitted between two electrodes and the potential difference is measured between two other electrodes (Figure 2.1). The ratio of voltage to current is the resistance that when multiplied by a factor taking into account the spacing between the electrodes, gives a parameter known as the apparent resistivity. When the measurement is made over a homogeneous surface, the apparent resistivity is equal to the true resistivity of the ground. However, when the resistance is made over a complicated subsurface structure, the apparent resistivity is a weighted average of the resistivities of the various rocks below the surface. The resulting apparent resistivity value depends on the subsurface structures. Resistivity distributions in the ground can be derived from the measured apparent resistivity values using inversion methods implemented, for instance, in commercially available software programs. The convention today is to perform a large number of four electrode measurements along profiles or over areas to achieve resistivity models as 2D sections or as 3D volumes, respectively. This is normally done using multi-electrode systems.

Generally, the imaging depth increases with increasing electrode distance. As a rule of thumb the penetration depth for a Schlumberger array is L/4 where L is the distance between two

outermost active current electrodes. For the Wenner array the penetration depth is around L/6 (Loke 2004). However, this is only the case if the sub-surface is a homogenous earth. The current will seek to obtain the lowest possible total resistance on the path between the two current electrodes. For example a very low resistive layer near the surface would prevent the current from penetrating deeper into the ground. In this case, the resolution of the deeper layer will be limited. By contrast, a very high resistivity layer close to the surface would force the current down to a less resistive layer. The depth of investigation therefore depends very much on the resistivity of the different layers as well as the largest electrode separation.

Usually, resistivity data are measured along 2D profiles. Assuming a 2D earth might in some cases be problematic. This would create 3D effects in the resistivity data, especially in this particular case where the geology is highly variable on a relatively small scale. In order to obtain the best 2D view, the profiles should be perpendicular to the geological structures.

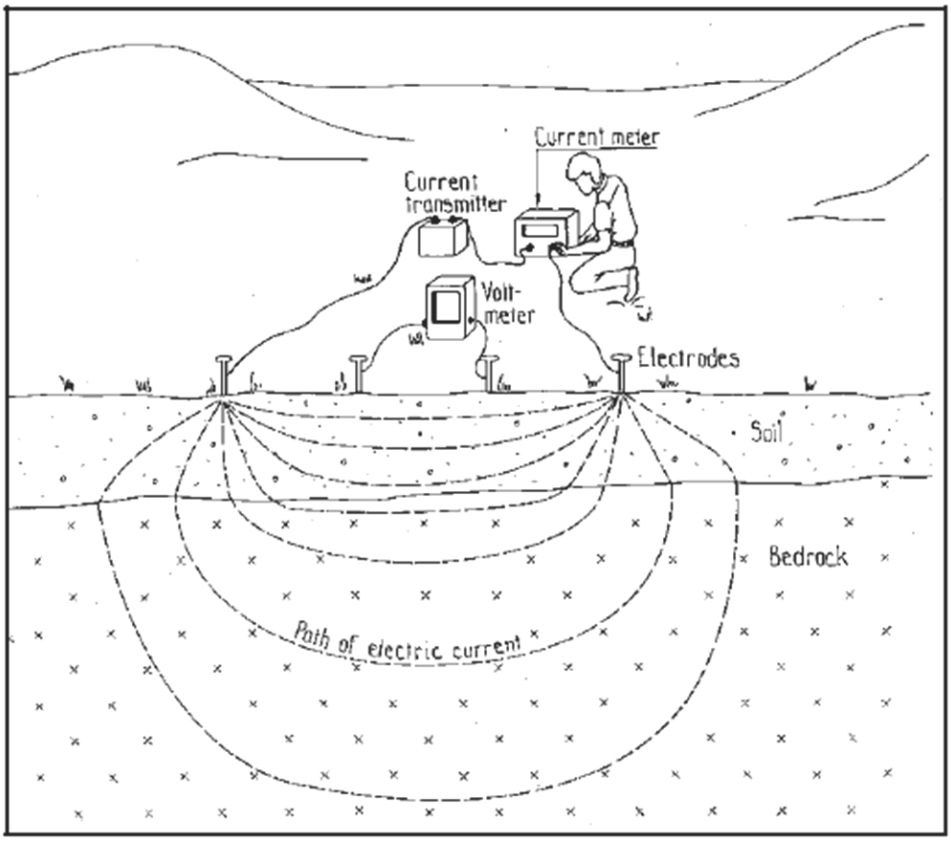

Figure 2.1. *Principles of resistivity surveying (Robinson and Coruh, 1988).*

2.1 Data acquisition

The ABEM Lund imagining system was used for data acquisition. It consists of a resistivity meter, a relay-matrix switching unit, two sets of electrode cables, a computer, steel electrodes power generator and various connectors (Figure 2.2). The cable sets are composed of 4 electrode cables, each with 21 take-outs and 200 meters length.

Figure 2.2. *The ABEM LUND Imaging System together with the Terrameter SAS 1000 / 4000 system.*

2.2 Vertical Electrical Sounding (CVES) method

The system allows for the so-called roll-along system (Fig. 2.3). Roll-along means that several multi-core electrode cables are rolled out along a straight line and moved successively, thus giving continuous profiles. This is a rapid approach for getting information about the spatial distribution of the resistivity in the sub-surface.

There are different electrode configurations for resistivity measurement which offer advantages and disadvantages compared to each other in terms of logistics and resolution, and the choice is usually a trade-off between these factors. In this study we used the so-called gradient array electrode configuration. This electrode configuration is well-suited for multi-channel data acquisition systems, so that many data-points can be recorded simultaneously for each current injection, so as to reduce fieldwork time significantly without compromising the data density (Dahlin & Zhou 2002).

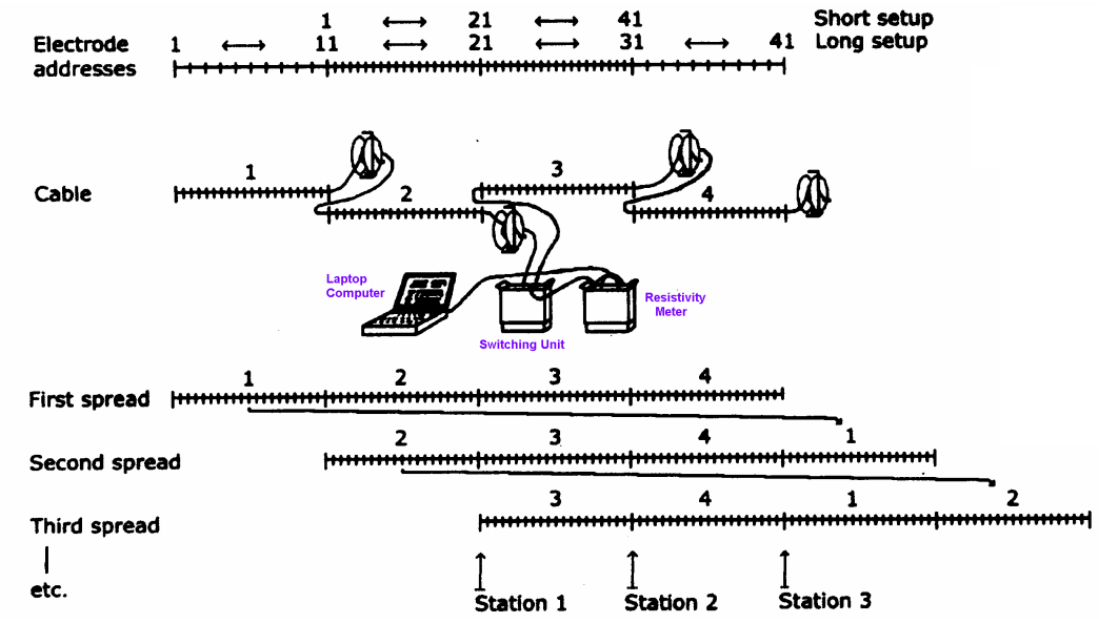

Figure 2.3. *Sketch outline of the ABEM Lund Imaging System. Each mark on the cables indicates an electrode position (Dahlin 1996). The cables are placed along a single line (the sideways shift in the figure is only for clarity). This figure also shows the principle of moving cables when using the roll-along technique.*

The combination of different layouts (GRAD4L8 and GRAD4S8) is intended for multiple gradient array CVES roll-along measurements, and has been found very useful for a variety of applications. The difference between the two is the layout length (Table 1). The layouts are defined as protocol files in the ABEM system (ABEM 2007, Manual instruction). It is important to select the protocol files when trying to set up the instrument in the correct order, starting with the long layout (GRAD4L8) before selecting the protocol for short layout (GRAD4S8). GRAD4S8 is designed to supplement GRAD4L8 for the shortest electrode spacings only. It gives a dense near-surface cover, and a slightly sparser measurement pattern at long electrode spacings. GRAD4LX8 is similar to GRAD4L8 but supplemented with expanding Wenner-Schlumberger measurements for the longest electrode separations in order to improve the data cover for the largest investigation depths (Figure 2.4).

Table 1 *Gradient array layout (ABEM 2007, Manual instruction)*

Array type	Protocol name	Address file	No of data ORG	No of data UP	No of data DWN	Total data for one layout
Gradient	GRAD4L(X)8	LONG	512(608)	248(340)	248(340)	1080
	GRAD4S8	SHORT	248	160	160	

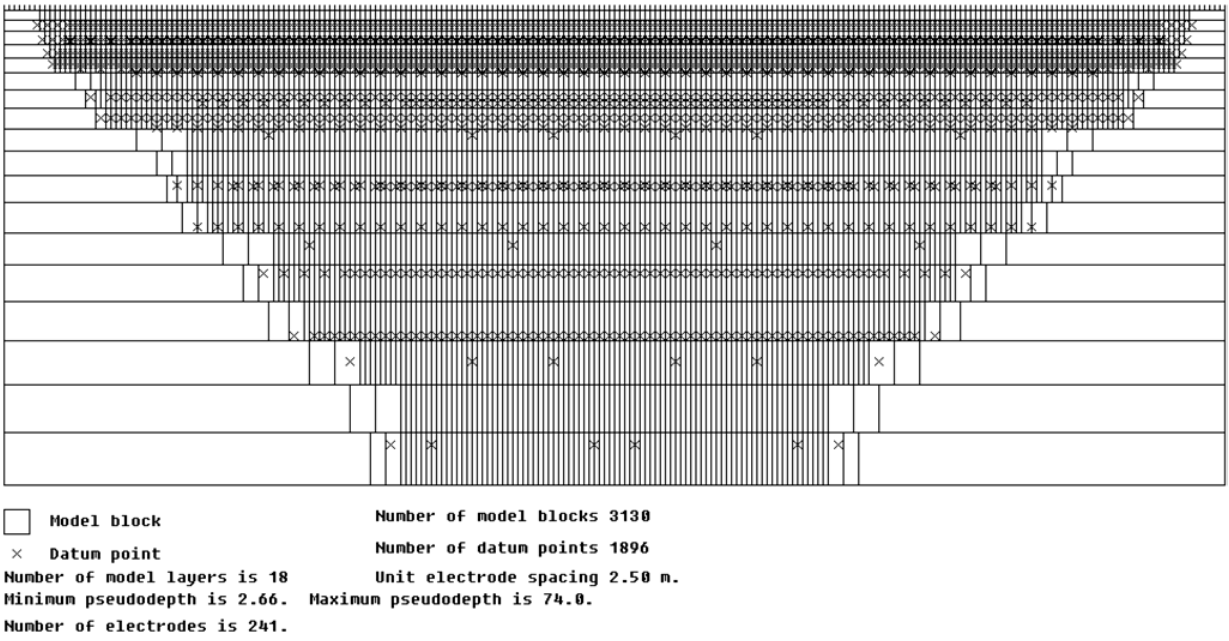

Figure 2.4. *Data cover of GRAD4L8 and GRAD4S8 for roll-along with three full stations (minimum electrode spacing 5 metres). Note that many data points fall on top of each other in multiple gradient array pseudosection plots (ABEM 2007, Manual instruction)*

2.3 Data acquisition

The measurements were conducted in 2007 and 2008. In total, seven profiles with a length between 800 and 1800 m were acquired in the study area (Fig. 2.5). Profile 1,4,5 and seven were measured in areas with rough topography, potentially dignostic of the message of fault segments of the MTFC. A typical site locality is shown from Profile 4 in Figure 2.6. GPS has been used for positioning, and the profiles are roughly orientated SSE to NNW, which is perpendicular to the assumed strike of the MTFC.

Figure 2.5. *Topographic map of the study area with location of the resistivity profiles (blue lines) and the refraction profile (dashed green line). See Figure 1. 1 for location of study area.*

Figure 2.6. *A typical location for the resistivity profiles.*

2.4 Processing of the 2D resistivity profiles

After the field survey, resistance measurements are usually reduced to apparent resistivity values. Practically all commercial multi-electrode systems come with the computer software to carry out this conversion. We processed and inverted the data by using the RES2DINV (version 3.55) software. This software lets the operator to have full control on data quality giving the possibility to remove bad data points to improve overall data quality. There are some causative sources for these bad data points, for example very poor ground contact at an electrode such that sufficient current cannot be injected into the ground, forgetting to attach the clip to the electrode, connecting the cables in the wrong direction, etc. As a general rule, before carrying out the inversion of a data set, we first take a look at the data as a pseudosection plot as well as a profile plot. The bad data points with noise show up as spots with unusually low or high values. In profile form, they stand out from the rest and can be easily removed manually for the data set. For example Figure 2.7 shows the data quality for Profile 2 in pseudosection form (Figure 2.7a) and in profile from (Figure 2.7b), the bad data that should be removed are also shown as red crosses in the figure. The problem of non-uniqueness is well known in the inversion of resistivity sounding and other geophysical data. For the same measured data set, there is wide range of models that can give similar calculated apparent resistivity values. We used traditional least square inversion method.

In surveys over areas with significant changes in ground surface elevation, the effect of the topography must be taken into account when carrying out inversion. The RES2DINV program can be used to incorporate the topography into the inversion model (Loke 2004).

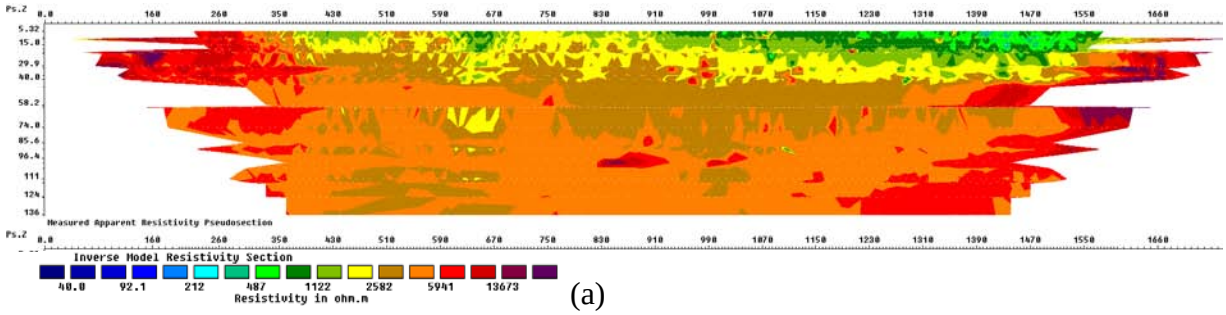

(a)

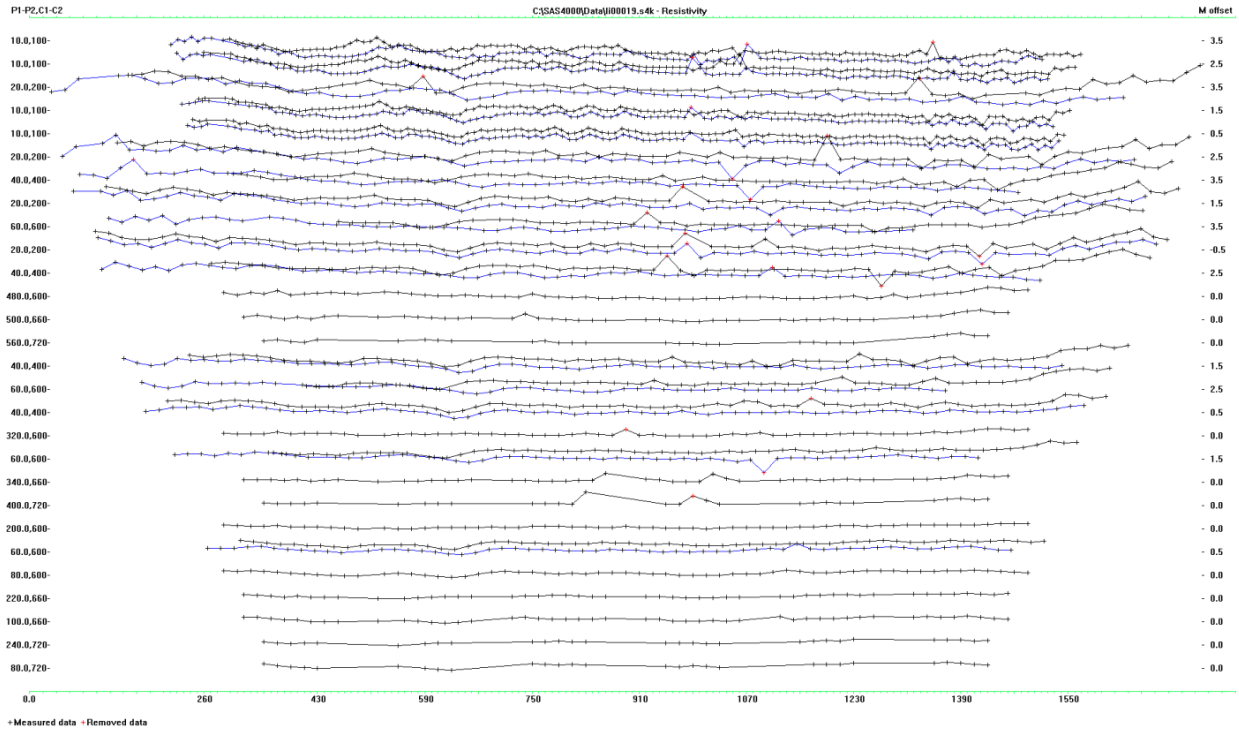

(b)

Figure 2.7. *Example of a field data set including some bad data points. The apparent resistivity data in (a) pseudosection form and in (b) profile form. Bad points that should be removed from data depicted as red crosses.*

Normally RES2DINV uses a model where the width of the interior model cells (Fig. 2.4) is the same as the unit electrode spacing. In some situations with large resistivity variations near the ground surface, this might not be sufficiently accurate. The model with a cell width of one unit electrode spacing has a maximum possible misfit of one half the electrode spacing for a near-surface inhomogeneity (Loke 2004). In some cases, this misfit can cause significant distortions in the lower sections of the inversion model. The cell size is too coarse to accurately model the

anomalies due to the small near-surface inhomogeneities. This forces the inversion program to distort the lower sections of the model in an attempt to reduce the data misfit. A finer model with a cell width of half the electrode spacing has a maximum misfit of one-quarter the unit electrode spacing, so the effect of the model cell boundary misfit should be much less. Using finer cells will lead to longer inversion times, so using a width of half of unit electrode spacing seems to provide the best trade-off (Loke 2004). Electrode spacing was 10 meters for all the profiles measured in study area. Unit electrode spacing was used for inversion of Profiles 6 and 7, while for the other profiles half of electrode spacing has been used.

2.5 Results of 2D resistivity survey

The results of the data inversion are shown in Figures 2.8 to 2.14.

2.5.1 Profile 1

The first profile has a length of 1000 meters and is located in between the mapped fault segments, but on relatively high elevation with a distinct topography. Four low resistivity zones can be detected by looking at the inverted data which are numbered (1) - (4) (Figure 2.8). The low resistivity zones (2) and (4) have a dip between 45 and 50 degrees towards the south. Low-resistivity zone (3) is almost vertical with a potential northern dip. Low resistivity zone (1) is located in the beginning of the profile and it dip is not resolved.

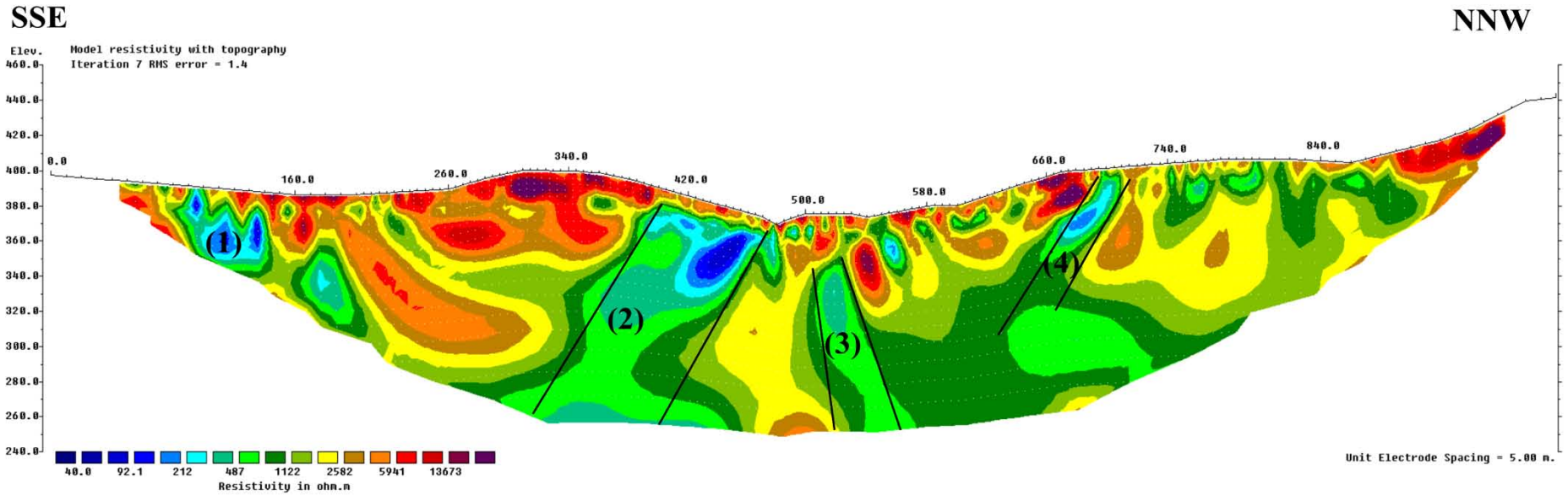

Figure 2.8. *Resistivity Profile 1. Numbers indicate the low resistive zones. See Figure 2.5 for profile location.*

2.5.2 Profile 2

The profile is 1800 meters long and located perpendicular to one of the main segments of the MTFC. The inverted data shows three low-resistivity anomalies and a pronounced low-resistivity layer at the top of the section (Figure 2.9). The latter corresponds to water saturated sediments. The numbered low resistivity anomalies on the profile relate potentially to weak zones due to the tectonic activity of the MTFC.

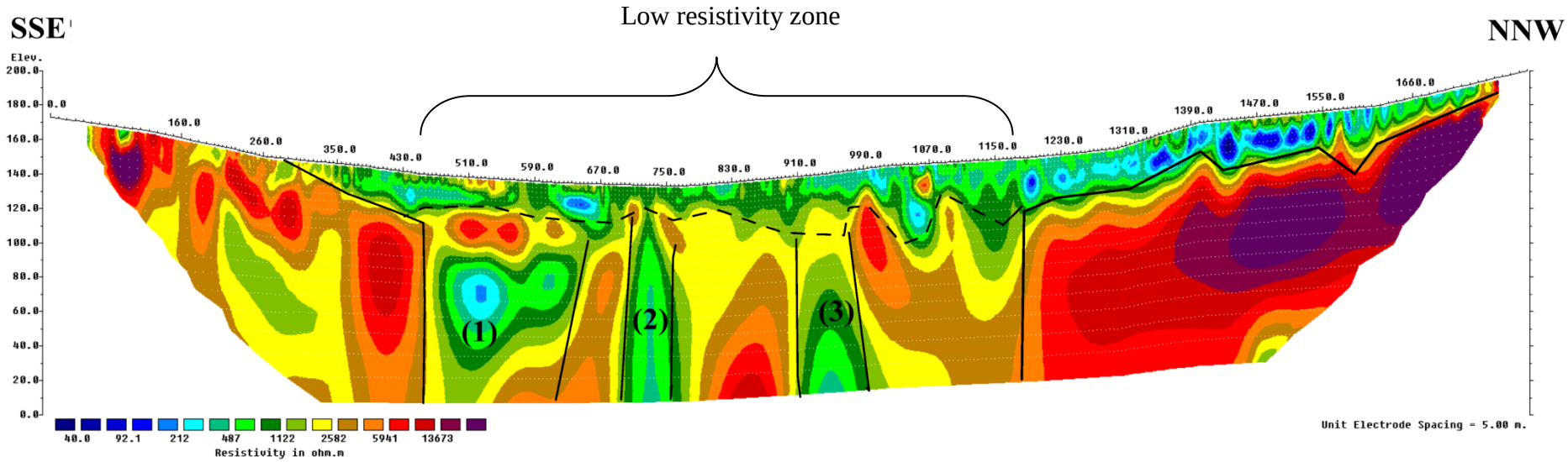

Figure 2.9. *Resistivity Profile 2. Numbers indicate the low resistive zones, the solid lines depict bedrock boundary and the dashed line represents the top of bedrock where is not well distinguishable. See Figure 2.5 for profile location.*

2.5.3 Profile 3

The profile has a length of 1400 meters and is an extension to the north of Profile 2. Except a shallow low-resistivity layer at the top, the resistivity along the profile is resistive and there is not an obvious anomaly that could be distinguished from the inverted data. This indicates that the MTFC is probably crossing to the south, at the location of Profile 2.

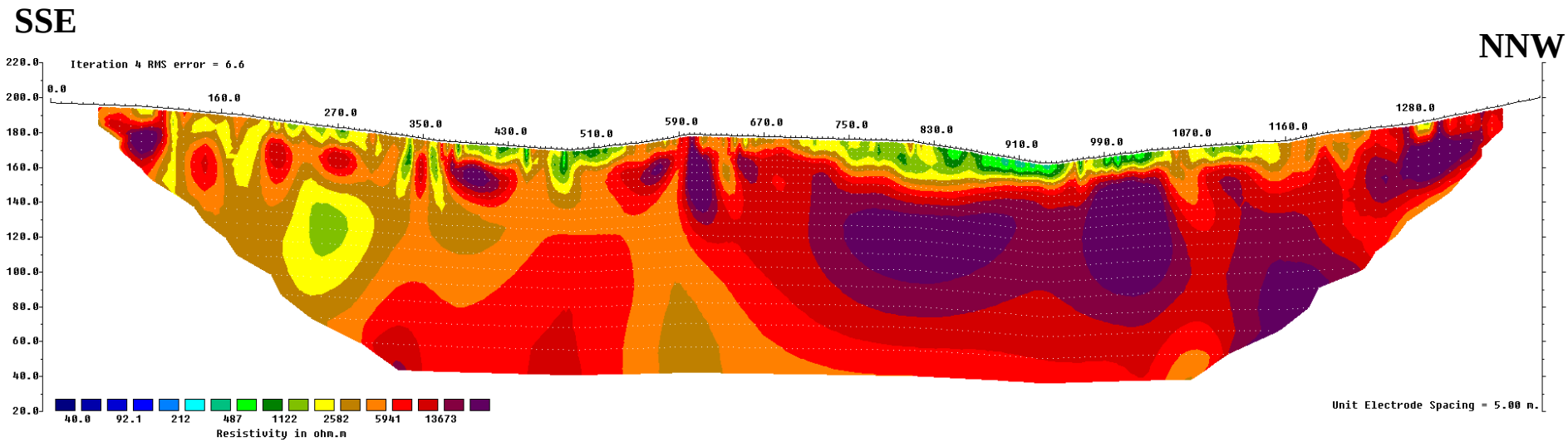

Figure 2.10. *Resistivity Profile 3. See Figure 2.5 for profile location.*

2.5.4 Profile 4

This profile is located at the eastern side of Tingvollfjorden and has a length of 800 meters. The profile is located in a depression (Figures 2.6 & 2.11). Between the northern and southern part a large resistivity contrast is observed, which can be interpreted as a signal related to the fault or a sudden contrast in lithology in the basement. An anomaly numbered (1) is probably is an artifact which comes from the limitation of the method where there is depression in the bedrock surface.

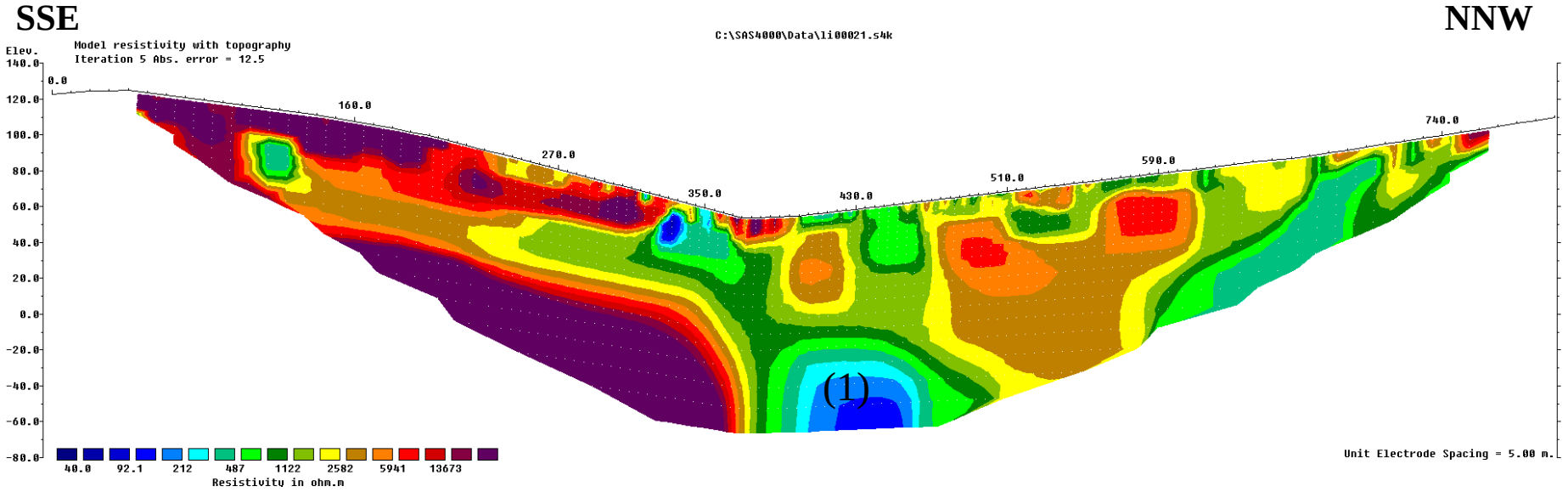

Figure 2.11. *Resistivity Profile 4. See Figure 2.5 for profile location.*

2.5.5 Profile 5

This profile is 1400 meters long and was carried out in a rough topography setting, and is prolongates Profile 4, but with a lateral offset of almost 1000m. The resistivity profile shows three very low anomalies: two of them are very shallow (No. (1) and (2) in Figure 2.12); The first low resistivity zones located in southern end of the profile which there no information about its extension to depth. The third zone is clearly extending to depth, but should be interpreted carefully, as it is located close to the lower boundary of the resistivity model. Both zones cannot be clearly linked to segments of the MTFC.

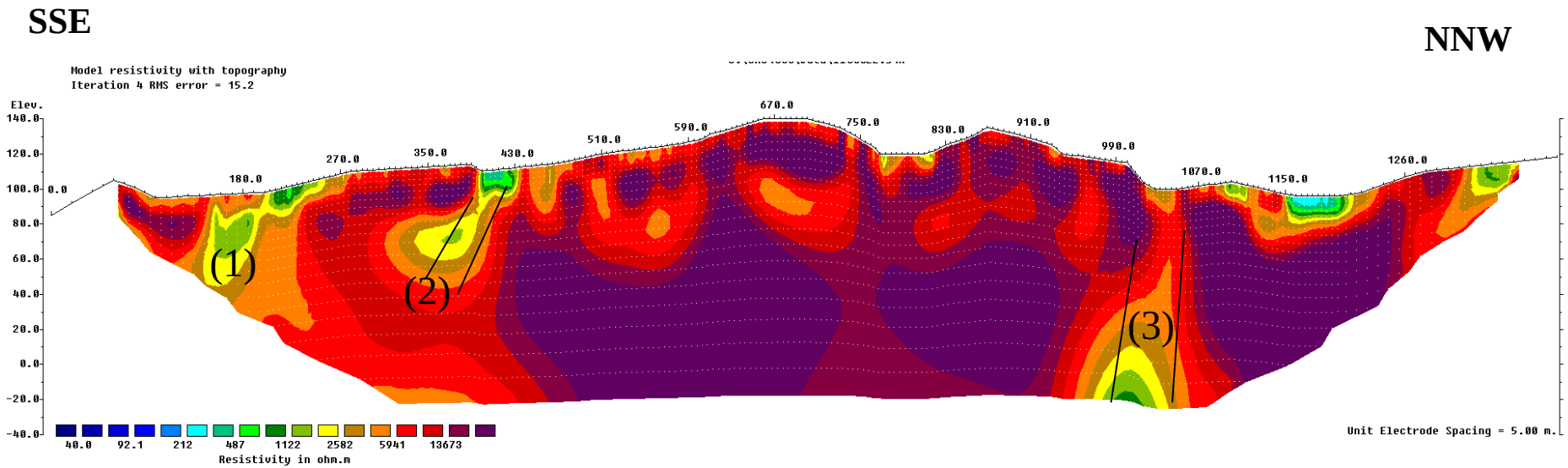

Figure 2.12. *Resistivity Profile 5. Numbers indicate the low resistive zones.See Figure 2.5 for profile location*.

2.5.6 Profile 6

Profiles 6 and 7 are located in the area of Eidsøra, where main geological and topographic evidence is given suggests a segment of the MTFC (Figure 2.5). Profile 6 has a length of 1400 m and a series of small-scale low resistivity anomalies. This implies many fractures and crushed zones in the bedrock. The profile is located along a road and we can correlate outcrops with the resistivity profile. The zones indicated by numbers 1, 2 and 3 are due to their width and depth extension, the most likely candidates for anomalies associated with segments of the MTFC.

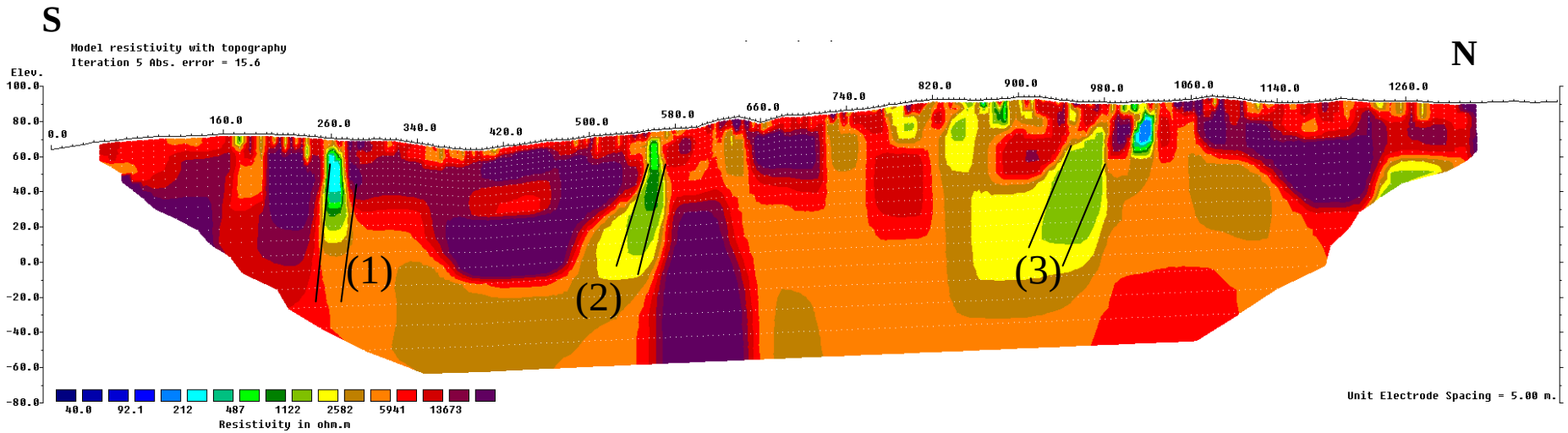

Figure 2.13. *Resistivity Profile 6. Numbers 1, 2 and 3 indicate the low resistive zones. See Figure 2.5 for profile location.*

2.5.7 Profile 7

The profile is almost an extension of Profile 6 with a slight lateral offset (Figure 2.5) and has a length of 1400 m. The resistivity profile shows a zone of low resistivity close to the surface, which represents water-saturated sedimentary or weathered layer. This layer is separated from high resistive bedrock by dashed line (compacted till; Figure 2.14). Low-resistivity zone (1) is located in the southern end of the profile which there no information about its extension to depth can be found. The other low resistivity zones show a means almost fault dip towards the southern part of the profile. Both zones can potentially be linked to weakness zones of the MTFC.

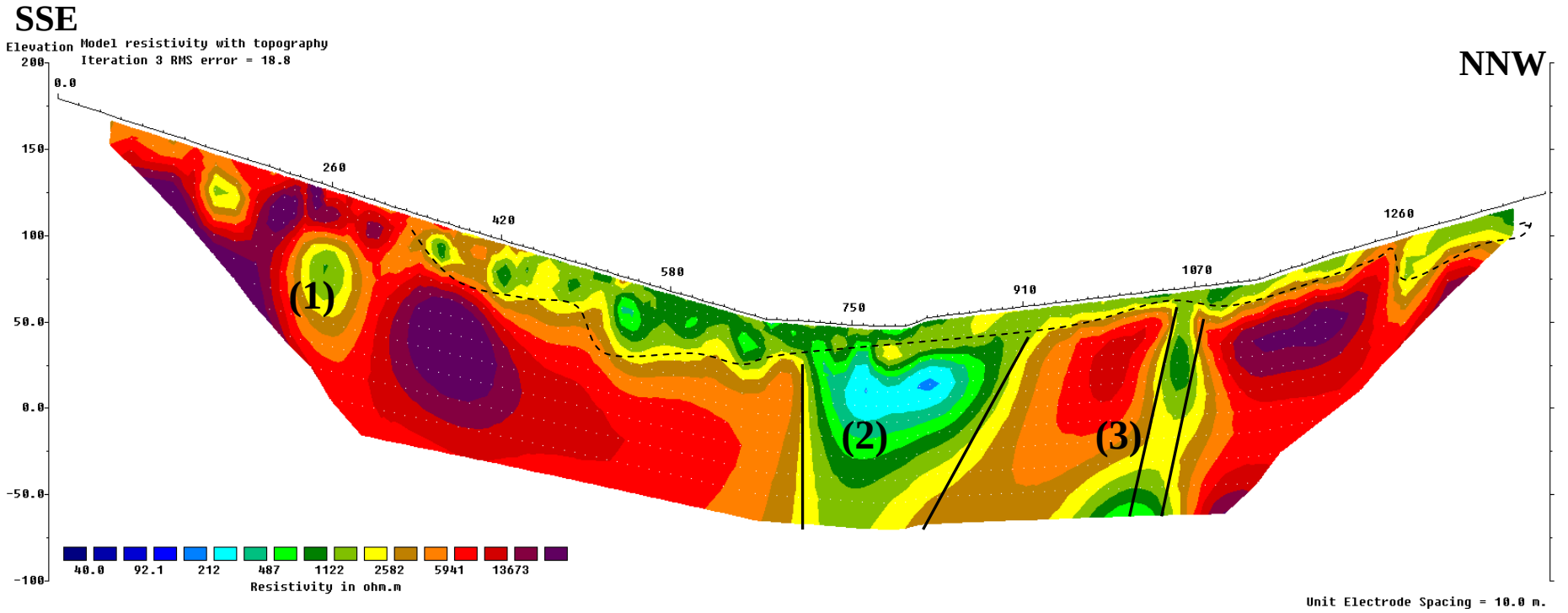

Figure 2.14. *Resistivity Profile 7. Numbers indicate the low resistive zones, solid lines depicted bedrock boundaries and the dashed line separates high resistive fresh bedrock from a low resistive sedimentary or weathered layer. See Figure 2.5 for profile location.*

3 REFRACTION SEISMICS

Similar to geoelectric measurements, also seismic experiments are often carried out in exploration geophysics. Refraction experiments are based on the times of arrival of the initial ground motion generated by a source recorded at different distances. Complications related to late arrivals in the recorded ground motion are discarded. Thus, the data set derived from refraction experiments consists of a series of times versus distances. These are then interpreted in terms of the depths to subsurface interfaces and the speeds at which motion travels through the subsurface within each layer. These speeds are controlled by a set of physical constants, called *elastic parameters* that describe the material. Any change in rock or soil property will cause seismic wave speed to change (Redpath 1973).

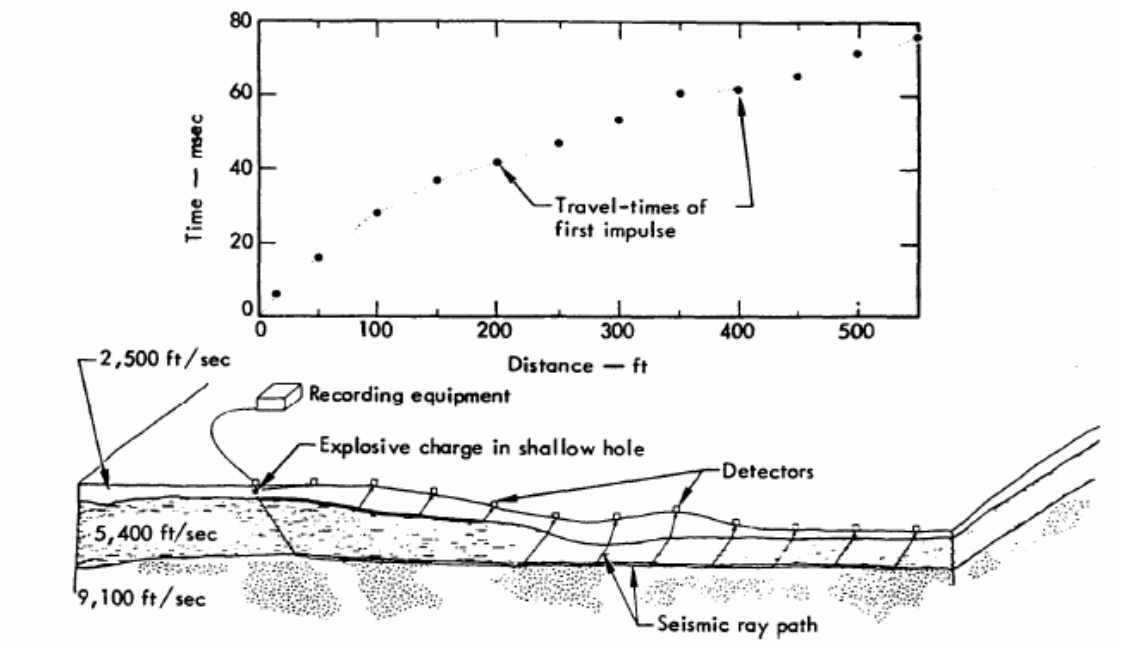

Figure 3.1. *Schematic diagram illustrating the shallow refraction seismic method (Redpath 1973)*

3.1 Field work

A 1320 m long refraction seismic profile with almost SSE to NNW strike was measured across the anticipated main fracture zone in the Eidsøra region, along resistivity Profile 7. The data was acquired in October 2007 with the seismic recording system ABEM TERRALOC MK6 with 24 channels (Figure 3.2). The profile was measured with two seismic cables, each with 12 geophone connections. Geophone spacing along the cables was 10 m, except at the end of the cables where the spacing was reduced to 5 m. To resolve dipping structures, it becomes necessary to carry out both forward and reverse shooting in order to determine all the parameters required to solve for the reflector geometry (Reynolds 1997).

Figure 3.2. *The seismic recording system ABEM TERRALOC MK6.*

Five shots were performed in each day of measurement with a distance of (1) 5 meters to the first geophone, (2) a shot 110 meters away from the first shot along the profile backward, (3) a shot 110 meters away from the first geophone, (4) a shot with 5 meters distance from the last geophone and finally (5) a shot located 110 meters away from the last geophone along the profile. This measuring system was repeated six times along the profile line to get full coverage of the length. Totally 32 shots points have been gathered along the profile. Energy source for the shootings was ordinary dynamite with electrical ignition. For short distances we used 100 grams of dynamite, for larger distances from the geophones up to 200 grams have been used. Table 2 lists the coordinates of the shot points and Figure 3.3 shows the shot locations.

Table 2 *Location of shot points along the seismic profile*

Shot points name on the map	Distance from starting point of profile (m)	WGS 84 (UTM zone 32) E	WGS 84 (UTM zone 32) N	Elevation (m)
A	-110	457548.00	6962649.00	204
B	-5	457500.00	6962735.00	177
C	110	457454.00	6962836.00	154
D	220	457406.00	6962938.00	132
E	330	457361.00	6963028.00	109
F	440	457328.00	6963125.00	88
G	550	457284.00	6963232.00	67
H	660	457236.00	6963333.00	52
J	770	457202.00	6963429.00	49
K	880	457171.00	6963524.00	55
L	990	457119.00	6963635.00	70
M	1100	457083.00	6963739.00	83
N	1210	457055.00	6963843.00	98
O	1320	457017.00	6963943.00	117
P	1370	457010.00	6963984.00	125

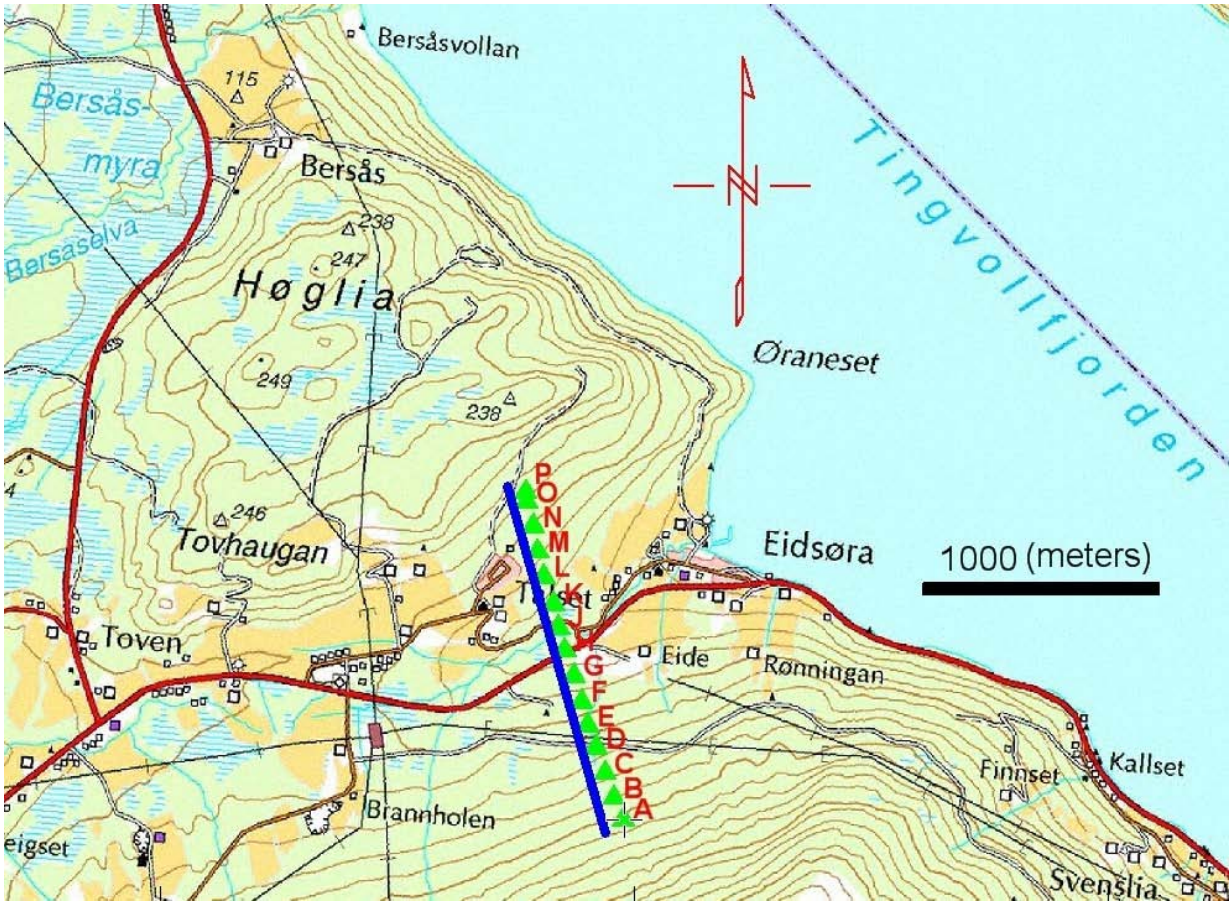

Figure 3.3. *Location of the refraction profile. The shot points are shown with green triangles. Letters refer to Table 2. The resistivity Profile 7 is shown in blue.*

3.2 Processing and interpretation of the refraction seismics

The first step in processing/interpreting refraction seismic data is to pick the arrival times of the signal, called first break picking. A plot is then made showing the arrival times against the distance between the shot and geophone. This is called a time-distance graph (Figure 3.4-3.9). The travel time curves are made by using the well-known ABC-method (Hawkins, 1961), which implies a systematic summation of arrival times from forward and reverse recordings. The method was originally based on a common point on the ground surface and two separate points on the refractor, yielding an average depth. The classical plus-minus method (Hagedoorn, 1959) is used for estimating seismic velocities and layer thickness in combination with estimating layering and thickness from intercept times and crossover distances. The interpretation based on these methods is shown in Figure 3.9.

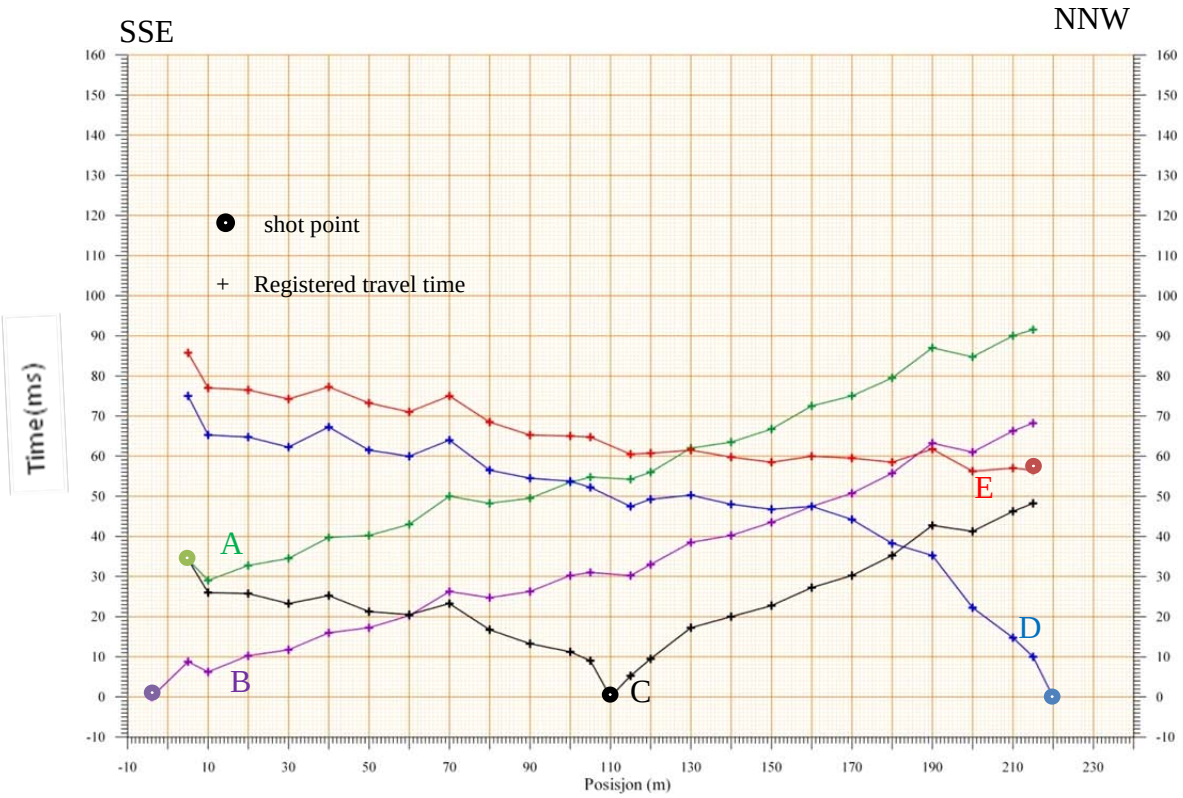

Figure 3.4*. Travel times from shot points for first lay out. Different colours show the recorded time for different shot points (see Table 2 and Figure 3.3). The horizontal axis shows the distance from the starting point of the profile.*

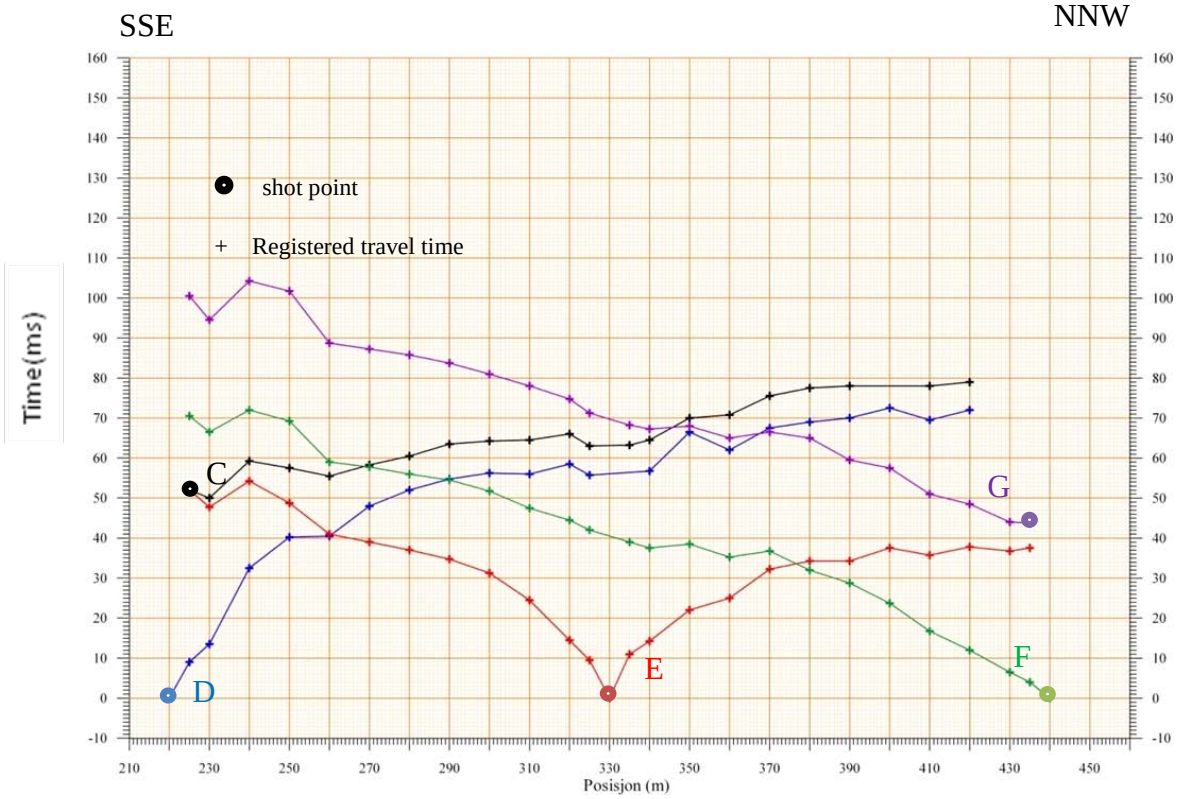

Figure 3.5. *Travel times from shot points for second lay out. Different colours show the recorded time for different shot points (see Table 2 and Figure 3.3). The horizontal axis shows the distance from the starting point of profile.*

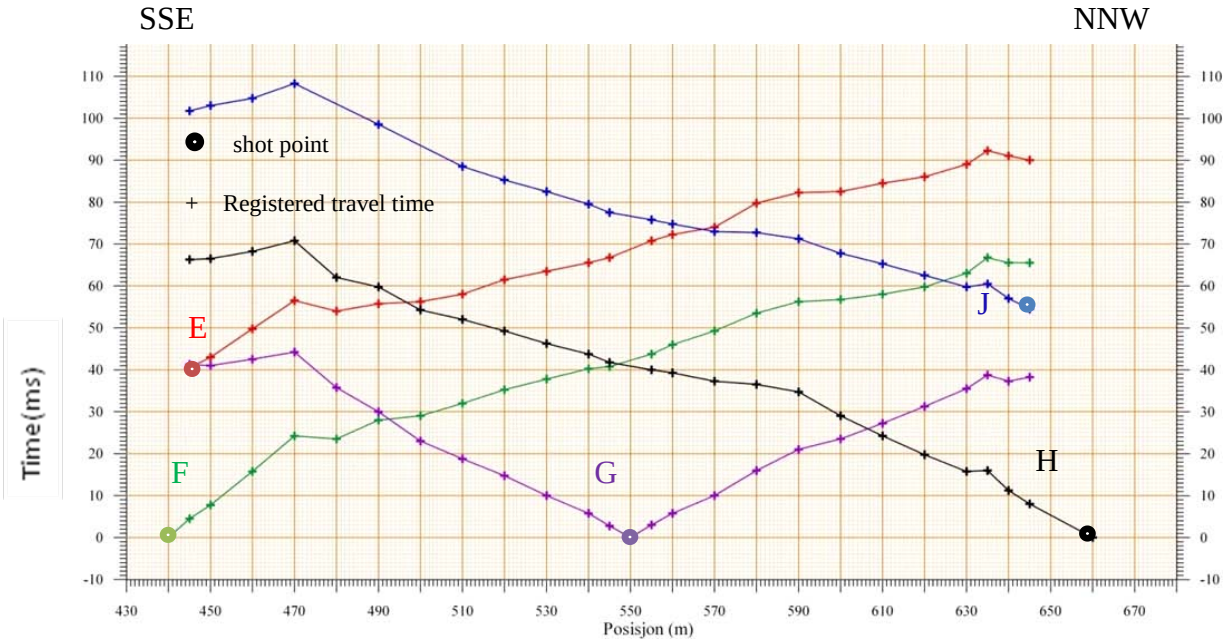

Figure 3.6*. Travel times from shot points for third lay out. Different colours show the recorded time for different shot points (see Table 2 and Figure 3.3). The horizontal axis shows the distance from the starting point of profile.*

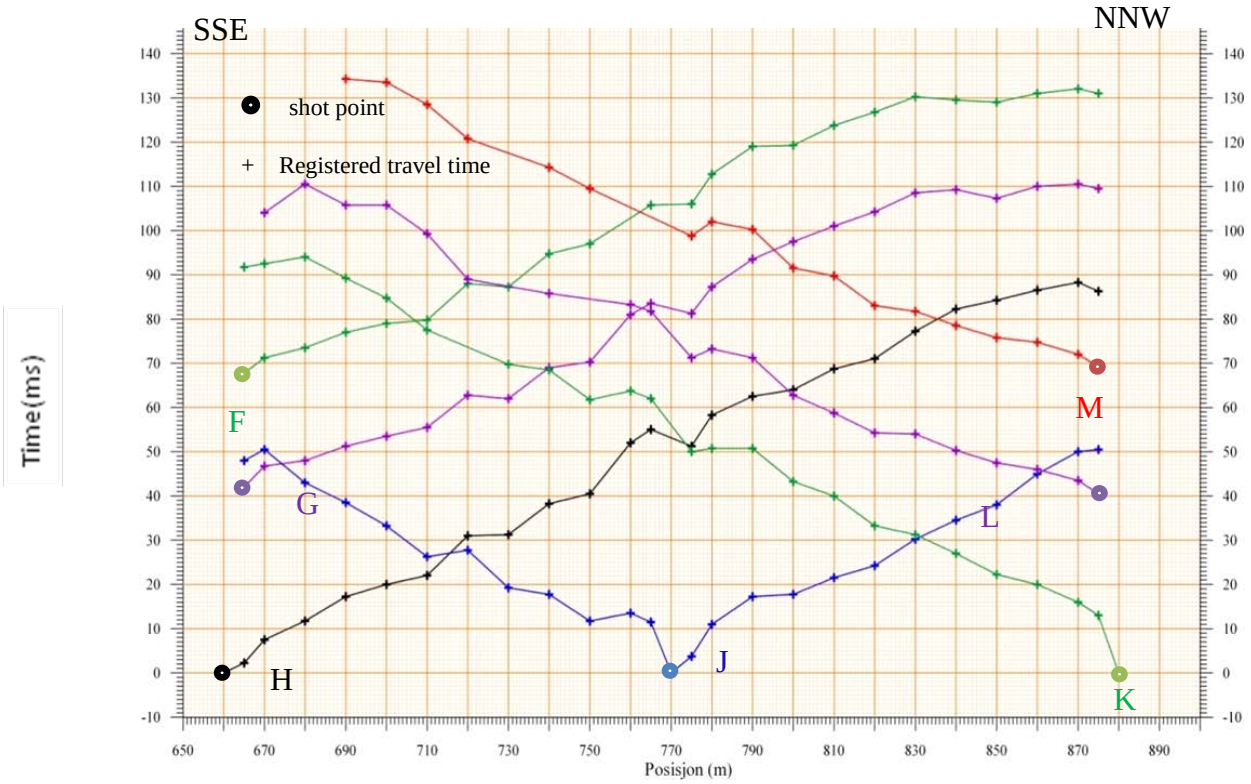

Figure 3.7 *Travel times from shot points for fourth lay out. Different colours show the recorded time for different shot points (see Table 2 and Figure 3.3). The horizontal axis shows the distance from the starting point of profile.*

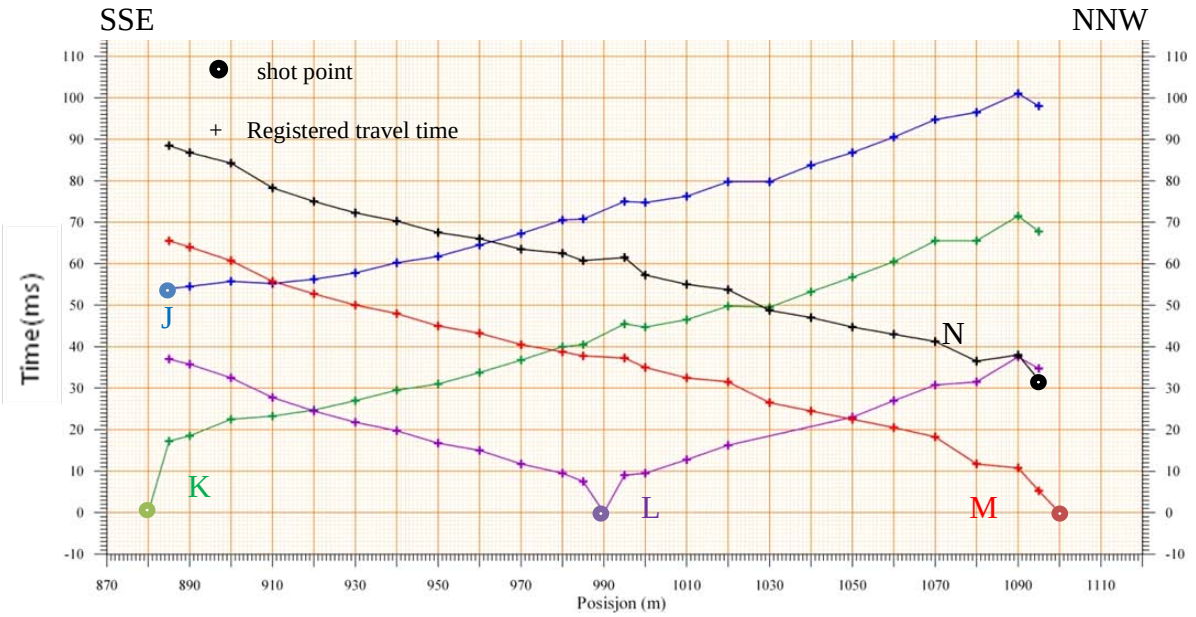

***Figure 3.8**. Travel times from shot points for fifth lay out. Different colours show the recorded time for different shot points (see Table 2 and Figure 3.3). The horizontal axis shows the distance from the starting point of profile.*

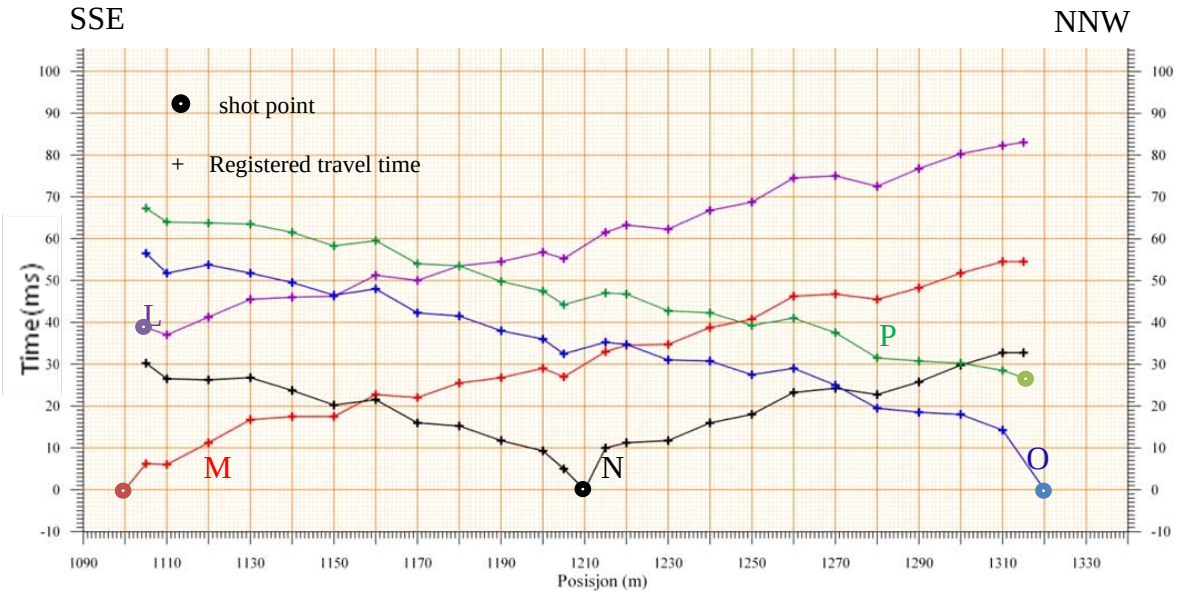

***Figure 3.9.** Travel times from shot points for sixth lay out. Different colours show the recorded time for different shot points (see Table 2 and Figure 3.3). The horizontal axis shows the distance from the starting point of profile.*

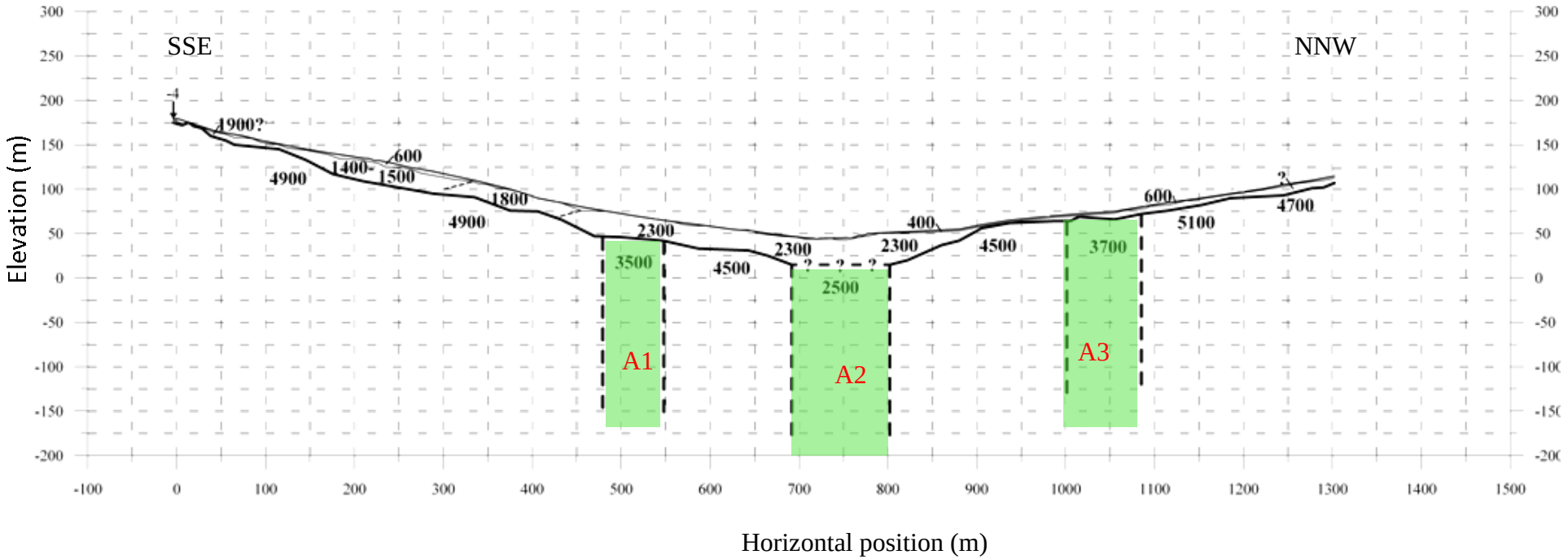

***Figure 3.10**. Interpreted section along the refraction profile. Velocities of layers are shown in bold numbers in m/s. The profile is corrected for terrain effects A1, A2 and A3 show the low velocity zones across the profile. The low velocity zones are interpreted to have vertical extension, as no information of the dip or the depth of extension can be obtained from our refraction experiment.*

The conducted shallow refraction profile has a length of 1300 m (Figure 3.10). The bottom of the valley has an elevation of44-45 m (asl) and is located 700-750 m from the starting point of the profile. The first point of the profile is located at height 179 m asl and the last point at 115 m (asl). The bedrock along the profile is covered by superficial deposits of different kinds and thickness. Horizontal distances from the starting point of profile will be used for describing all anomalies and specific positions.

Three different layers can be distinguished in the seismic interpretation (Fig. 3.10). At the top a layer of 0.5-5.0 m thickness with very low seismic velocity (400-600 m/s) exists, which represent dry deposits of sand/gravel or loose till. In some places this layer is dominated by swampy bog and peat. In the underlying bedrock seismic velocity is very variable. Along the central lower part of the profile (450-900 m) the velocity is about 2300 m/s, which could relate to very compact till. Towards the south the velocity is 1800 m/s and decreases to 1400-1500 m/s between 150 and 320 m. The highest value is interpreted as till-dominated deposits, while the lower values can relate to sorted material of sand and gravel (glaciofluvial deposits). The total thickness of the superficial deposits between position 155 m and 870 m along the profile is varying from 15 to about 30 m. In the northern part of the profile the thickness varies from 3 to max. 12 m, and the smallest values are shown at position 905-940 m. Seismic velocity in the third layer which is interpreted as bedrock is varying from 2500 to 5100 m/s. Low values (less than 4000 m/s) indicate areas of fractured or crushed bedrock.

There are indications of three distinct low-velocity zones in the bedrock denoted as A1-A3 along the profile. The main zone (with velocities as low as 2500 m/s) is about 110 m wide and is located below the central part of the profile (position 690-800 m). The very low velocity is caused by intensive fracturing and crushing of the bedrock. Another zone is located 200 m north of the main zone and is about 80 m wide (position 1000-1080 m). The seismic velocity is estimated to 3700 m/s and indicates less fracturing than in the main zone. A similar zone is located about 140 m south of the main zone (position 430-550 m) with a width of 70 m and a seismic velocity of 3500 m/s. The seismic velocity of the bedrock in between the low- velocity zones is about 4500 m/s, while it is 4900 m/s in the southern part of the profile and 4700-5100 m/s in the northern part.

4 DISCUSSION AND CONCLUSIONS

In this survey 2D resistivity survey has shown that it is able to constrain the vertical extent of fracture-zones. The method also images the width and resistivity of the fracture-zone close to the surface, but at the deeper levels, the zone will appear to be wider with higher resistivity. The dip of fracture zone may also be estimated (e.g. profiles 2 and 7). Depression in the bedrock surface might be falsely interpreted as a fracture-zone and artificial effects are common (e.g. profile 4). The resistivity profiles 1-7 show a series of very low resistive zones, which can be related to fractures in the bedrock or the fault segments. For example, Profile 5 shows a very deep low-resistivity zone in between very high resistive zones. Such an anomaly can be caused by a water-saturated fracture or a brecciated rock within a fault core. Such anomalies have been observed on different profiles and can probably be used to trace the fault through the study area.

The seismic profile shows also weak zones with very low P- wave velocity. These weak zones probably related to the Tjellefjorden fault strand of the MTFC. Figure 4.1 shows a correlation between resistivity Profile 7 and the refraction results. By comparing the two we can easily distinguish the overburden from the bedrock. However, only two of the three zones imaged by the seismic profile correlate to anomalies in the resistivity profile. This can be related to the following: depth to bedrock can be estimated in both methods; however, in refraction seismics the boundary of overburden and bedrock is very sharp where in 2D resistivity it is not so clear. The seismic anomaly A1 does not correlate to an anomaly in the resistivity profile. This anomaly can be a typical blind zone in refraction seismics. Westerdahl (2003), demonstrated with synthetic models how such anomalies can be created by shallow cavities, and limit the use of the refraction method here.

Two zones show a very nice correlation. The low-velocity zone A2 is estimated to have a width of 100 m, but has a width of 200 m in the resistivity profile. Although, we are not able to estimate the bottom depth of these anomalies, both methods show that these anomalies can be traced in very shallow subsurface. In fact, the resolution of the resistivity method decreases exponentially with depth and the image becomes increasingly fuzzier with depth. Generally we can conclude that we succeeded in our surveys to detect two segments of MTFC in an area covered by Quaternary deposits.

By comparing resistivity Profiles 2 and 7 it can be seen that the low resistivity zone corresponds to the Fannefjorden Fault is 3 times wider than the zone related to the Tjellefjorden Fault. In the next step, we will try to use geological sampling and magnetic studies to trace the fault between the different profiles here. Gravity data might furthermore help us to estimate the thickness of the overburden and to distinguish amphibolitic structures, which have a distinct signal in the gravity and magnetic field, but no direct relation to segments of the Møre-Trøndelag Fault Complex.

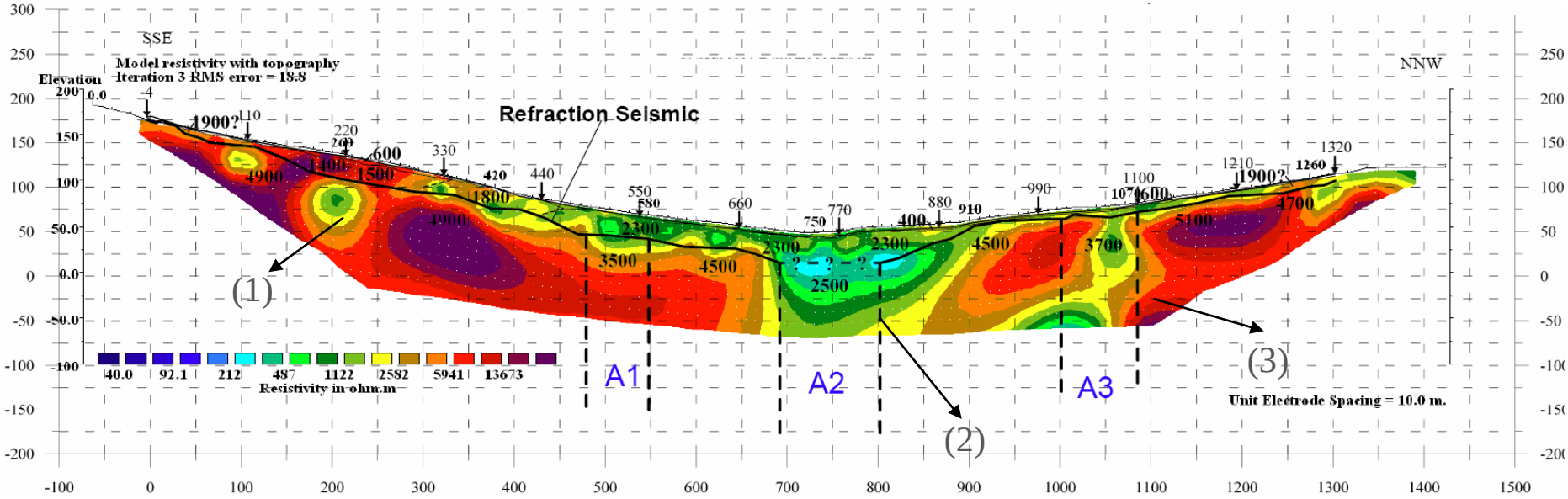

Figure 4.1. *Overlay of the refraction seismic on resistivity profile 7. A1, A2 and A3 shows low velocity zones along the refraction profile and (1), (2) and (3) show low resistivity anomalies in the 2D resistivity section.*

5 ACKNOWLEDGEMENTS

The presented study is part of the project “The Møre-Trøndelag Fault Complex - an integrated study” funded by the Research Council of Norway and the Geological Survey of Norway. We thank Jan Steinar Rønning for discussions on the data processing, and Tim Redfield and Christophe Pascal for discussion and comments on the geological implications.

6 REFERENCES

ABEM 2007: Instruction Manual, ABEM Terrameter SAS 1000/4000, ABEM Printed Matter No 93109 http://www.abem.se

Binley, A. and Kemna, A., 2005: DC resistivity and induced polarization methods *in* Hydrogeophysics: Rubin, Y. and Hubbard, S., Eds., Springer.

Dahlin, T., 1996: 2D resistivity surveying for environmental and engineering applications. First Break, 14, 275-284.

Dahlin, T., Bjelm, L., and Svensson, C., 1999: Use of electrical imaging in site investigations for a railway tunnel through the Hallandsås Horst, Sweden: *Quarterly Journal of Engineering Geology*, 32**,** 163-172.

Dahlin, T. and Zhou, B., 2002: Gradient and mid-point-referred measurements for multichannel 2D resistivity imaging, *Procs. 8th Meeting Environmental and Engineering Geophysics, Aveiro, Portugal, 8-12 September 2002*, 157-160.

Ganerød, G. V., Rønning, J.S., Dalsegg, E., Elvebakk, H., Holmøy, K., Nilsen, B. and Braathen, A. 2006: Comparison of geophysical methods for sub-surface mapping of faults and fracture zones in a section of the Viggja road tunnel, Norway. Bull Eng Geol Env (2006) 65: 231 – 243). ISSN: 1435-9529 (Paper) 1435-9537 (Online)

Hagedoorn J.G. 1959: The plus-minus method of interpreting seismics refraction sections. Geophysical Prospecting 7, 158-182.

Hawkins, L.V., 1961: The Reciprocal method of routine shallow seismics refraction investigations: *Geophysics*, **26**, 806–819.

Loke, M. H., 2004: Tutorial: 2-D *and 3-D electrical imagining surveys*. 136 p

Parasnis, D. S., 1997: *Principles of Applied Geophysics*: Chapman and Hall.

Redfield, T.F., Osmundsen, P.T. 2009, The Tjellefonna fault system of Western Norway: Linking late-Caledonian extension, post-Caledonian normal faulting, and Tertiary rock column uplift with the landslide-generated tsunami event of 1756, Tectonophysics, 474, 106–123.

Redfield, T.F., Braathen, A., Gabrielsen, R.H., Osmundsen, P.T., Torsvik, T.H., & Andriessen, P.A.M., 2005: Late Mesozoic to Early Cenozoic components of vertical separation across the Møre–Trøndelag Fault Complex, Norway. *Tectonophysics*, 395, 233– 249.

Redpath, Bruce B., 1973: Seismics refraction exploration for engineering site investigations, U.S. Army Engineer Waterways Experiment Station Explosive Excavation Research Laboratory, Technical Report E-73-4, Livermore, California, 51 p.

Reynolds, J. M., 1997: An Introduction to Applied and Environmental Geophysics: John Wiley & Sons.

Robinson, E. S. and Coruh, C., 1988: *Basic exploration geophysics,* Wiley.

Rønning, J.S., Dalsegg, E., Elvebakk, H., & Storrø, G., 2003: Characterization of fracture zones in bedrock using 2D resistivity. 9th EEGS European Meeting, Prague, August 31 – September 4 2003.

Westerdahl, H., 2003: Modellering av seismiske data over løsmassefylte depresjoner, svakhetssoner og ved kabelheng. Norges Geotekniske Institutt . Intern rapport, nr.2338.